Engineering Conferences International
ECI Digital Archives

The 14th International Conference on Fluidization – From Fundamentals to Products

Refereed Proceedings

2013

Study on Relationship between Fluidization Characteristics and Lateral Force Acting on Two Contacting Particles

Azri Bin Alias
Okayama University of Science, Japan

Kenya Kuwagi
Okayama University of Science, Japan

Hiroyuki Hirano
Okayama University of Science, Japan

Toshihiro Takami
Okayama University of Science, Japan

Jonathan Seville
University of Surrey, UK

STUDY ON RELATIONSHIP BETWEEN FLUIDIZATION CHARACTERISTICS AND LATERAL FORCE ACTING ON TWO CONTACTING PARTICLES

Azri Bin Alias[1], Kenya Kuwagi[1*], Hiroyuki Hirano[2],
Toshihiro Takami[1] and Jonathan Seville[3]

[1] Okayama University of Science
Department of Mechanical Systems Engineering
1-1 Ridai-cho, Okayama 700-0005, Japan
[2] Okayama University of Science
Department of Biotechnology and Applied Chemistry,
1-1 Ridai-cho, Okayama 700-0005, Japan
[3]University of Surrey
Faculty of Engineering and Physical Sciences,
Guildford, Surrey, GU2 7XH, United Kingdom
*T: +81-86-256-9574; F: +81-86-255-3611; E: kuwagi@mech.ous.ac.jp

ABSTRACT
In order to clarify the fundamental mechanism of fluidization behaviors, i.e., bubbling and homogeneous fluidizations, small scale phenomena such as drag force and other particle-fluid interaction forces around the particles were examined. In the present study, we analyzed the flow around two contacting particles. The flow was calculated using the body-force type Immersed Boundary (IB) method. We focused on the lateral force acting on each particle laterally with respect to the flow direction, i.e., the direction of the drag force. It was determined that a bubble is formed by a horizontal force acting on particles, i.e., a lateral force. Accordingly, the lateral force is one of the important factor in bubble formation. The results were plotted as dimensionless values.

INTRODUCTION
Fluidization behavior can vary drastically with the fluidization velocity and the particle and fluid properties. The characteristics of fluidization of the powder presented by Geldart (1) are classified into four types according to the particle size and particle density or the difference in fluid density. This is also generally known as Geldart's powder classification chart. Geldart's powder classification chart classifies particles into group C, A, B, and D in ascending order of particle size. The characteristic of the particles can be classified simply as follows:

Group C: Cohesive, high interparticle force that leads to difficulty in fluidization and may form channels and slugs.
Group A: Can be homogeneously fluidized under a specified condition. A bed may expand before bubbling. The frequency of fragmentation of bubbles is high
Group B: Fragmentation of bubbles is predominant compared to coalescence.
Group D: Can be classified by the slow bubbles that appear in a fluidized bed.

Moreover, a number of studies on the mechanism of the difference between the homogeneous and bubbling fluidizations have been performed using stability

analysis. In a homogeneous fluidization study, Rietema and Musters (2) reported that the surface of a homogeneously fluidized gas bed was tilted, and a more detailed study by Gilberson and Yates (3) revealed that the effect was due to non-vertical flow of gas. These studies indicate that fluid-dynamics phenomena can account for a wide spectrum of behavior in an unstable heterogeneous bed, but not in stable homogeneous systems.

Recently, DEM simulation has been used for this problem. Homogenous fluidization of Geldart A particles has been studied by Mao et al. (4), who found that the homogeneous fluidization regime represents a quasi-equilibrium state in which the force level exists at the macroscopic level rather than at the individual level. Di Renzo et al. (5) studied the transition from the homogeneous regime to the bubbling regime in gas and liquid fluidized beds through DEM-CFD simulations. Simulations were carried out for the water fluidization of micron glass and cohesionless alumina for B and A particles. They found that air fluidized alumina powder exhibited a transition from a homogeneous regime to a bubbling regime, which is in quantitative agreement with the theory of the stability of the homogeneous bed state.

Studies on bubbling behavior have also been conducted by Davidson and Harrison (6). For example, they studied fast or slow bubbles that appear in a fluidized bed and examined their mechanisms using their proposed model and through analysis of the gas flow around a bubble.

A number of studies have been conducted in order to clarify the mechanism behind the differences between the homogeneous and bubbling fluidizations. Although there have been a number of analyses on the underlying mechanism of fluidization, the basic mechanisms have not yet been sufficiently clarified. The purpose of the present study is to clarify the relationships between the flow characteristics and the lateral force. Moreover, a number of studies have examined macroscopic phenomena. In the present study, we focus on particle size and microscopic phenomena and behavior, and a numerical simulation was conducted in order to analyze the fluid flow around two contacting particles and to measure the force acting on the particles.

NUMERICAL ANALYSES

In the present study, we used the Immersed Boundary (IB) method which is a direct numerical simulation in a multi-phase flow. We used the body-force-type immersed boundary method proposed by Kajishima et al., (7) for the numerical procedure because this method provides a simple numerical procedure. The governing equations are given below.

As an example, in order to study the fast or slow bubbles that appear in a fluidized bed, the mechanisms have been examined through the analysis of gas flow around a bubble.

Fluid phase

The equations for mass and momentum conservation are as follows:

$$\nabla \cdot u_f = 0 \qquad (1)$$

$$\frac{D\vec{u}_f}{Dt} = -\frac{1}{\rho_f}\nabla p + \vec{f}_{vis} + \vec{f}_{ib} + \vec{g} \quad (2)$$

where $\vec{f}_{ib}$ is the body force term which makes the velocity in a fluid cell occupied by a particle equal to the velocity of the particle. In the present simulation, the following equation, which was proposed by Kajishima et al. (7), was used:

$$\vec{f}_{ib} = \varepsilon_p(\vec{v}_p - \vec{u})/\Delta t \quad (3)$$

The particle volume fraction ε_p at a computational cell including a fluid-particle interface was calculated using the method involving a sub-mesh system proposed by Tsuji et al. (8).

Particle phase

The equations of motion of a particle in the translational and rotational directions are as follows:

$$\frac{d(m_p\vec{v}_p)}{dt} = -\rho_g\int_{V_p}\vec{f}_{ib}dV + \sum_{j\neq i}\vec{F}_{nij} + m_p\vec{g} \quad (4)$$

$$\frac{d(\vec{I}_p\cdot\vec{\omega}_p)}{dt} = -\rho_g\int_{V_p} r\times\vec{f}_{ib}dV + \left(\sum_{j\neq i}\vec{F}_{tij}\right)\cdot r_p \quad (5)$$

where the second term on the right-hand side of Equation 4 denotes the particle-particle interaction force, i.e., the collision force in the normal direction to the particle surface at the contact point. The second term on the right-hand side in Equation 5 denotes the particle-particle interaction moment. Moreover, $\vec{f}_{tij}$ is the contact force in the tangential direction, and r_p is the radius of the particle. The numerical simulations are explained by Kuwagi et al. (9).

ANALYSIS CONDITION

The problem schematic and the analysis domain are shown in Fig. 1. The fluid flow was injected at a constant rate from the bottom of the analysis region. At the center of the analysis region, two particles are fixed and brought into contact for the numerical analyses. The region for calculation is shown on the right-side of the figure.

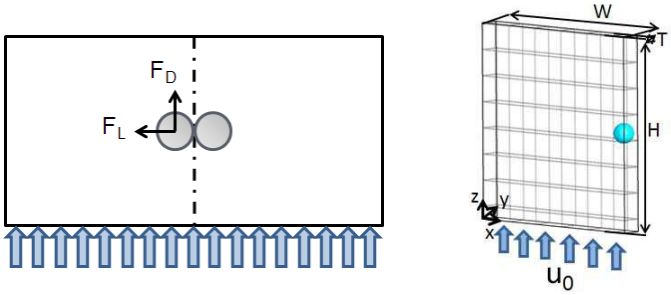

Fig. 1 Problem schematic and analysis region

In the present study, we focused on the effect of the lateral force on Geldart's powder classification (1). The lateral force was non-dimensionalized by the drag

force on the buoyancy force in the analyses.

Note that since the analysis condition ranges over only low Reynolds numbers, the flow was assumed to be symmetrical. Since the fundamental effect of a flow on the fluidization behaviors were distinguished by Geldart's powder classification, cohesive forces such as Van der Walls force that are actually acting on the group C particle are not taken into account in the present study.

NUMERICAL PROCEDURE

In the present numerical analyses, time discretization was approximated by an explicit method and the inertial terms by the third-order up-wind scheme. The pressure distribution was solved with the HS-MAC (SOLA) method. The boundary conditions for the simulations are as follows:

$$u_x = 0, \frac{\partial u_y}{\partial x} = \frac{\partial u_z}{\partial x} = 0 \qquad \text{at } x = 0,\ W \qquad (6)$$

$$u_y = 0, \frac{\partial u_x}{\partial y} = \frac{\partial u_z}{\partial y} = 0 \qquad \text{at } y = 0,\ T \qquad (7)$$

$$u_x = u_y = 0, u_z = u_0 \qquad \text{at } z = 0 \qquad (8)$$

$$\frac{\partial u_x}{\partial z} = \frac{\partial u_y}{\partial z} = \frac{\partial u_z}{\partial z} = 0 \qquad \text{at } z = H \qquad (9)$$

Equation 7 was used because the effect of particle arrangement on the calculation of the drag force assumes that the flow is two-dimensional. The slip condition was used for the side planes, as indicated by Equation 6. The simulated results were examined in the terms of lateral force F_L compared with drag force F_D and the buoyancy force F_B, which is defined as follows:

$$F_B = \left(\rho_p - \rho_f\right)\bar{g}A \qquad (10)$$

Fig. 2 shows a flow regime map (10) plotted in terms of the Reynolds number and the Archimedes number (Re_p −Ar), which are defined as follows:

$$\mathrm{Re}_p = \frac{u\rho_f d_p}{\mu} \qquad (11)$$

$$Ar = \frac{d_p^3 \rho_f \left(\rho_p - \rho_f\right)\bar{g}}{\mu} \qquad (12)$$

The figure indicates the area of the fixed bed, homogenous fluidization, and bubbling fluidization. The results of the numerical simulation are also plotted in Fig. 2. The dotted line indicates that the area of homogeneous and bubbling fluidization changed with the pressure and heat, even for the same fluid.

The simulation conditions are listed in Table 1. The main fluids used in the present analyses are air and water. Air at 0.1 MPa (ordinary pressure), 1 MPa and 10 MPa was simulated. Heated air at 500°C was also simulated. The width and height of the analysis region are ten times larger than the particle diameter,

whereas the thickness of the analysis region is the same size as the particle diameter. The grid size used in the analysis is $\Delta x = \Delta y = \Delta z = 1/20 d_p$.

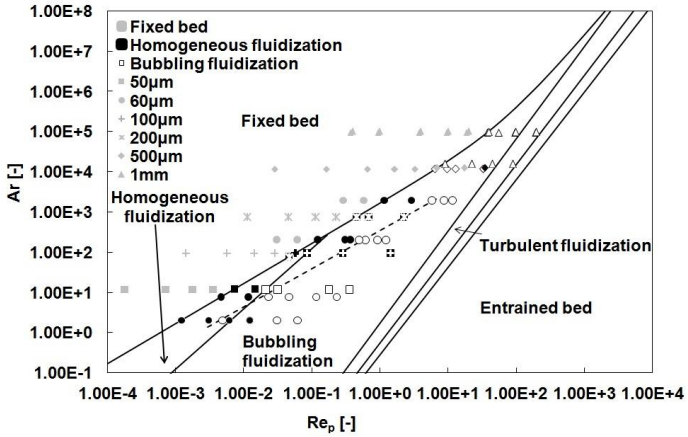

Fig. 2 Flow regime map

Table 1 Simulation conditions for drag and lateral force

Fluid	Viscosity (Pa•s)	Density (kg/m^3)
Air (0.1 MPa)	1.82×10^{-5}	1.20
Air (1 MPa)	1.82×10^{-5}	12.0447
Air (10 MPa)	1.82×10^{-5}	120.447
Air (500 ^{o}C)	3.55×10^{-5}	0.456085
Water	1.00×10^{-3}	998

The simulation conditions for various particle sizes are Group A, Group B and Group D particles. For the numerical simulation, water was used as a fluid, and glass bead (1 mm) and lead (1 mm) were used as size D particles.

DIMENSIONLESS GOVERNING EQUATIONS

Based on the present analyses, the dimensionless equations derived using the Hellums and Churchill (11) method was used. The equations are as follows:

Particle phase

$$\frac{d\vec{v}}{dt} = \frac{1}{\rho_p}\nabla p + \frac{1}{\rho_p V_p}\left(F_{pp} + F_{pf}\right) + \left(1 - \frac{\rho_f}{\rho_p}\right)g \quad (13)$$

The above equation is changed to the following dimensionless equation:

$$\frac{d\vec{V}}{dT} = \frac{1}{\rho^*}\nabla p + \left(\tilde{F}_{pi} + \tilde{F}_{pf}\right) + \frac{1}{\rho^*}\cdot\frac{Ar}{\mathrm{Re}^2} \quad (14)$$

Fluid phase

$$\frac{\partial \varepsilon}{\partial t} + \frac{\partial}{\partial x_j}\left(\varepsilon u_j\right) = 0 \quad (15)$$

$$\rho_f \frac{\partial}{\partial t}\left(\varepsilon u_i\right) + \rho_f \frac{\partial}{\partial x_j}\left(\varepsilon u_i u_j\right) = -\varepsilon\frac{\partial p}{\partial x_i} + f_{pi} + \rho_f \varepsilon g \quad (16)$$

The above equations are changed to dimensionless equations as follows:

$$\frac{\partial \varepsilon}{\partial T}+\frac{\partial}{\partial X_j}\left(\varepsilon U_j\right)=0 \qquad (17)$$

$$\frac{\partial}{\partial T}\left(\varepsilon U_i\right)+\frac{\partial}{\partial X_j}\left(\varepsilon U_i U_j\right)=-\varepsilon\frac{\partial P}{\partial X_i}+\tilde{f}_{pi}+\frac{\varepsilon}{Fr^2} \qquad (18)$$

$$\rho^*=\frac{\rho_p}{\rho_f},\ X_i=\frac{x_i}{d_p},\ X_j=\frac{x_j}{d_p},\ \vec{V}=\frac{\vec{v}}{u_o},\ P=\frac{p}{\rho_f u_o^2},\ T=\frac{tu_o}{d_p},\ K=\frac{k}{\rho_p d_p u_o^2},$$

$$\Delta=\frac{\delta}{d_p},\ H=\frac{\eta}{\rho_p d_p^2},\ D_p=\frac{d_p}{d_p},\ U_i=\frac{u_i}{v_o},\ U_j=\frac{u_j}{v_o},\ \tilde{F}_{pi}=\frac{\vec{F}_{pi}}{F_o},\ \tilde{F}_{pj}=\frac{\vec{F}_{pj}}{F_o},$$

$$\tilde{F}_o=\frac{\pi}{6}\rho_p d_p^2 U_o^2,\ \tilde{f}_{pi}=\frac{1}{\mathrm{Re}}\left\{\frac{3}{4}C_D\left(V-U\right)\frac{1-\varepsilon}{D_p^2}\varepsilon^{-2.7}\,\mathrm{Re}^{0.687}\times\frac{1}{\Delta X\Delta Y\Delta Z}\right\}$$

RESULTS AND DISCUSSIONS

Fig. 3 shows the relationship between the ratio of the lateral force to drag force and the Reynolds number. In comparing the results with the flow regime map in Fig. 2, the results were plotted according to the differences in the fluidized state. Gray represents the fixed bed. Black indicates homogeneous fluidization, and white indicates bubbling fluidization. As shown in the graph, homogeneous fluidization occurred in the low-lateral-force region, and the bubbling fluidization occurred in the high-lateral-force region.

In the high-lateral-force region, bubbles occurred because of the larger forces between the particles that are pushed away. On the other hand, in the low-lateral-force region, there is insufficient force between the particles that are pushed away, which results in a homogenous fluidized bed.

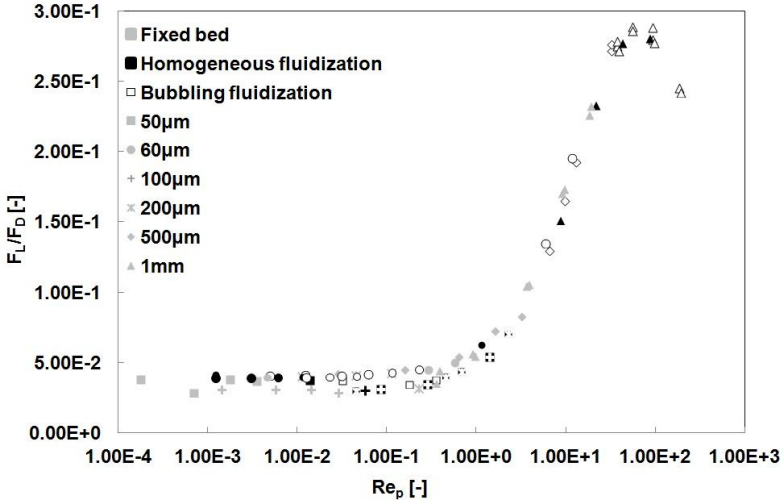

Fig. 3 Ratio of drag to lateral force

Based on these results, in the region in which F_L/F_D increased rapidly, the lateral force is related to the flow characteristics. However, ~~for liquid systems,~~ homogenous fluidization occurred at the high Reynold's numbers in liquid phase. On the other hand homogeneous fluidization in gas phase occurred at low-lateral-force region. From this result, we cannot conclude that the flow characteristics cannot be explained using only lateral and drag force.

Since the flow characteristics remain unclear, we attempted to verify the influence using the lateral and buoyancy forces as shown in Fig. 4. The graph shows that, as the Reynold's number increases in either condition, F_L/F_B also increases. At a low gradient, the plotted area consists primarily of Group A particle in homogenous fluidization. At a high gradient, the plotted area is mainly plotted by group B and Group D particles in bubbling fluidization. However, from the graph, the gradient plotted for the liquid phase is almost the same as the gradient for the Group D particle in gas phase. Accordingly, we still cannot explain the homogenous and bubbling fluidizations.

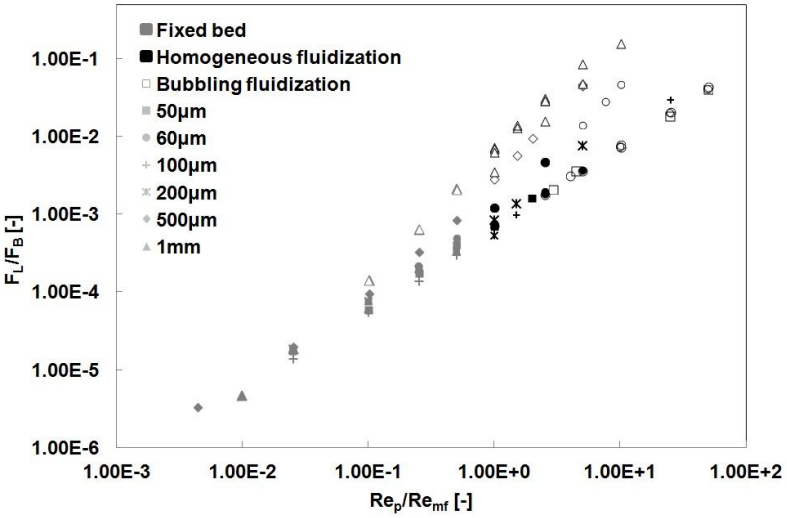

Fig. 4 Ratio of buoyancy to lateral force

From the dimensionless equation derived using the Hellums and Churchill method, the dimensionless lateral force F_L/F_0 is shown in Fig. 5, in which the fixed bed is shown in gray, the homogenous fluidization is shown in black and bubbling fluidization is shows in white.

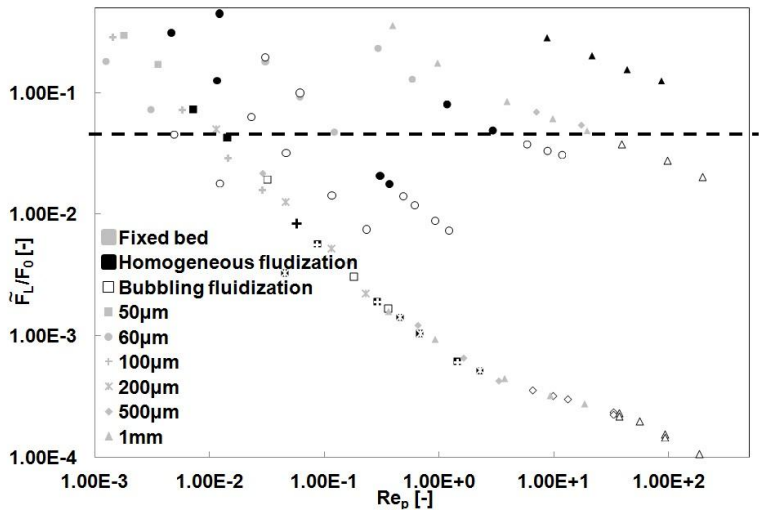

Fig. 5 Dimensionless Lateral Force

The graph shows that separate lines were plotted for each condition. The dashed line separates the fluidization state between the homogeneous and bubbling fluidizations. The upper dashed line shows the homogenous fluidization

state and the lower dashed line shows the bubbling fluidization state. Using the dimensionless lateral force derived by Hellums and Churchill method, the homogeneous and bubbling fluidizations were classified successfully.

CONCLUSION

In order to analyze the bubble behavior, which is one of the most important phenomena in a fluidized bed, small-scale phenomena, such as the drag force and other particle-fluid interaction forces around the particles, should be examined. The analysis revealed that the lateral force increased rapidly with respect to the drag force around the region Re_p between 0.1 and 1. The lateral force that occurred between particles can be considered to be related to the flow and bubbling characteristics. Based on the obtained results, the fluidization state was distinguished by the dimensionless lateral force F_L/F_D.

ACKNOWLEDGMENT

This present study was supported by the Ministry of Education, Cultural, Sports, Science and Technology of Japan through the Financial Assistance Program for the Social Cooperation Study (2012-2016).

REFERENCES

1 Geldart, D., Types of Gas Fluidization, Powder Technol., 7, 285-292, 1973.

2 Rietema, K. and Musters, S.M.P., The effect of interparticle forces on the expansion of a homogeneous gas-fluidized bed, Proc. Int. Symp. Fluidization and its Applications., Toulouse, France (1973)

3 Gilberson, M.A. and Yates, J.G., Bubbles, jets, X-rays and nozzle: what happens to fluidized beds under pressure., Ints. Chem. Eng. Jubilee Research Events, 433 (1997)

4 Mao, Y., Van Der Hoef, M. A., and Kuipers, J. A. M., Discrete Particle Simulation of the Homogeneous Fluidization of Geldart A Particles, Proceedings of Fluidization XI, Naples, Italy, (2004)

5 Di Renzo, A., P. Di Maio. F., Homogeneous to Bubbling Regime Transition in Gas and Liquid Fluidized Beds Through DEM-CFD Simulations, Proceedings of Fluidization XII, Vancouver, Canada, (2007)

6 Davidson, J. P. and Harrison, D. Fluidized Particles, Cambridge University Press, Cambridge, England, (1963)

7 Kajishima, T., Takiguchi, S., Hamasaki, H. and Miyake, Y., Turbulence Structure of Particle–Laden Flow in a Vertical Plane Channel Due to Vortex Shedding, *JSME Int. J. B.*, 44-4, (2001)

8 Tsuji, T., Narutomi, R., Yokomine, T., Ebara, S. and Shimizu, A., Unsteady Three-Dimensional Simulation of Interactions Between Flow and Two Particles, Int. J. Multiphase Flow, 29, (2003)

9 Kuwagi, K., Y. Shimoyama, Bin Alias, A., H. Hirano and T. Takami, “Examination of Various Estimation Equations for Drag Force by Using Immersed Boundary Method”, J. Chem. eng.,45-2,(2012),107-113

10 Horio, M., Circulating Fluidized Bed, J. R. Grace, A. A. Avidan and T. M. Knowlton (eds), Chapter 2, Blackie A and P, London, (1997)

11 Hellums,J.D.and Churchill,S.W. Applied Numerical Methods, Krieger Publishing, Malabar, Florida, pp. 319-461 (1964)